crystals

MDPI

Review

Thermodynamic Modeling and Mechanical Properties of Mg-Zn-{Y, Ce} Alloys: Review

Mohammad Aljarrah [1,2,*], Jasim Alnahas [2] and Mohammed Alhartomi [3]

[1] Industrial Engineering Department, Faculty of Engineering, The Hashemite University, P.O. Box 330127, Zarqa 13133, Jordan
[2] Industrial Engineering Department, Faculty of Engineering, University of Tabuk, Tabuk 71491, Saudi Arabia; jalnahas@ut.edu.sa
[3] Electrical Engineering Department, Faculty of Engineering, University of Tabuk, Tabuk 71491, Saudi Arabia; amalhartomi@ut.edu.sa
* Correspondence: maljarrah@hu.edu.jo

Abstract: Magnesium alloys are a strong candidate for various applications in automobile and aerospace industries due to their low density and specific strength. Micro-alloying magnesium with zinc, yttrium, and cerium enhances mechanical properties of magnesium through grain refinement and precipitation hardening. In this work, a critical review of magnesium-based binary systems including Mg-Zn, Mg-Y, Mg-Ce, Zn-Y, and Zn-Ce is presented. Based on the CALPHAD approach and first-principles calculations, thermodynamic modeling of Mg-Zn-Y and Mg-Zn-Ce ternary phase diagrams have been summarized. The influence of micro-alloying (yttrium and cerium) on the mechanical properties of magnesium is discussed. A comparison between mechanical properties of magnesium commercial alloys and magnesium–zinc–{yttrium and cerium} have been summarized in tables.

Keywords: thermodynamic modeling; magnesium; phase diagram; liquidus projection

Citation: Aljarrah, M.; Alnahas, J.; Alhartomi, M. Thermodynamic Modeling and Mechanical Properties of Mg-Zn-{Y, Ce} Alloys: Review. *Crystals* **2021**, *11*, 1592. https://doi.org/10.3390/cryst11121592

Academic Editor: Wojciech Polkowski

Received: 8 December 2021
Accepted: 15 December 2021
Published: 20 December 2021

1. Introduction

The need for weight reduction in automobile and aerospace industries makes magnesium alloys attractive due to their low density and high strength-to-weight ratio [1–3]. However, the use of magnesium alloys in structural parts is limited because of their poor mechanical properties at elevated temperatures [4–16]. Many researchers investigated the effect of micro-alloying on magnesium to enhance its mechanical performance [17–76]. The addition of rare-earth (RE) elements are attractive and receive increasing attention because of their excellent properties such as better creep resistance, grain refinement, improved ductility, enhanced formability, and strength [40,43–45,54,55,60,61,67–72,76].

Micro-alloying magnesium with RE such as zinc and yttrium resulted in promising mechanical properties [27,31,35,40,44,46,55,58,60]. RE elements enhance mechanical properties due to precipitation hardening through precipitation of nanoparticles of ternary phases [27–71]. These phases have an ability to inhibit the growth of deformation twins [18–23]. Furthermore, the addition of RE elements to Mg-Zn promote activation of prismatic slip and increase the stacking fault energy, therefore weakening the texture of magnesium alloys [35–40,44,51,61,66,72]. Micro-alloying magnesium with zinc increases its fluidity in casting [77], whereas yttrium addition has a remarkable effect on aging precipitation and high solid solution strengthening [78–80]. Moreover, cerium tends to precipitate a thermally high stable compound (Mg_2Ce) in magnesium rich region, which improve microstructure stability at elevated temperatures. Diluting zinc in Mg-Ce alloy significantly improves stretch formability by modifying the basal plane texture through solid solution hardening mechanism [81–85]. Moreover, the highest zinc in Mg-Ce alloy improves yield strength and ultimate tensile strength through precipitation of intermetallic

compounds. Whereas the ratio of Ce/Zn increases, grain refinements and loss of formability occurs [71,81–88]. Mg-Zn-Y alloys display promising mechanical properties because of precipitates of thermally stable ternary compounds (W-Mg_3Y solid solution, I-Mg_3YZn_6, and LPSO-phase $Mg_{12}ZnY$) as well as high solubility of yttrium in magnesium.

To better understand phase stability, phase relation, and the effect of precipitation on age hardening, knowledge of binary and ternary phase diagrams is essential. Additionally, accurate prediction of phase diagram plays an important role in materials development and alloy design. Phase diagram is a tool used to predict the equilibrium phase(s) and phase(s) percentage at certain temperatures for specified alloys and simulate the phase consistency and solidification process of individual alloys. Moreover, the percentage of the predicted phase(s) that exist in the microstructure can be calculated. This will enable us to track particular alloys during solidification and subsequent heat treatment by predicting phase composition and distribution. Therefore, binary sub-systems of Mg-Zn-{Y, Ce} including Mg-Zn, Mg-Y, Mg-Ce, Zn-Y, and Zn-Ce phase diagram have been critically reviewed. In addition, ternary phase diagrams of Mg-Zn-Ce and Mg-Zn-Y have been assessed. A comparison between mechanical properties of commercial Mg-based alloys and Mg-Zn-{Ce,Y} alloys has been reported.

The CALPHAD approach is a well-known method to predict phase equilibria in a multi-component system based on Gibbs free energy of the phases [89–91]. Solid solutions were modeled using compound energy formalism with sublattice [92]. The modified quasi-chemical (MQC) solution model precisely describes short-range ordering in the liquid phase; therefore, liquid phase was optimized using MQC to treat configurational entropy [93]. The main novelty of the current work is to critically review phase equilibria of Mg-Zn-{Y, Zn} systems and mechanical properties based on the experimental investigations reported in the literature.

2. Zinc-Yttrium Phase Diagram

Chiotti et al. [94] largely examined phase diagram and thermodynamic data of Zn-Y phase diagram using DTA, metallographic, and XRD. Mason and Chiotti [95] subsequently reviewed the work of [94] and measured phase relation and thermodynamic properties of the intermetallic compounds using eight samples. In the work of [94,95], tantalum containers were unsuccessful because of the penetration of Y-Zn liquid at high zinc contents. Mason and Chiotti [95] reported three intermetallic compounds that melt congruently: YZn, YZn_2, and Y_2Zn_{17} ($YZn_{8.5}$) at 1105, 1080, and 890 °C, respectively. Thermodynamic modeling of Y-Zn binary phase diagram in the work of [96–98] presented a polymorphic transformation in the YZn_2 at 750 °C, which is in accord with [95,99]. Mason and Chiotti [95] found five intermetallic compounds that decompose peritectically: YZn_3, Y_3Zn_{11} ($YZn_{3.67}$), $Y_{13}Zn_{58}$ ($YZn_{4.46}$), YZn_6, and YZn_{12} at 905, 896, 882, 872, and 685 °C, respectively. Mason and Chiotti [95] determined the thermodynamic properties of the intermetallic compounds using dewpoint method. The large number of intermetallic compounds found in the RE-Zn system was similar and related to RE-coordination number [100]. Crystal structure data of Y-Zn compounds were determined by [100–103]. Gibbs energy of formation of the intermediate compounds in the Y-Zn system was investigated by [104–108]. The most accurate description of Y-Zn binary phase diagram was established by Zhu and Pelton [109] based on experimental data [94,95] as shown in Figures 1 and 2. The optimized Y-Zn phase diagram presented by Zhu and Pelton [109] presented some amendment to the work of Spencer et al. [98]. The calculated enthalpy and Gibbs energies of formation of the intermetallic compound presented in the work of [98] are in good agreement with the experimental data of [95,104,105,108].

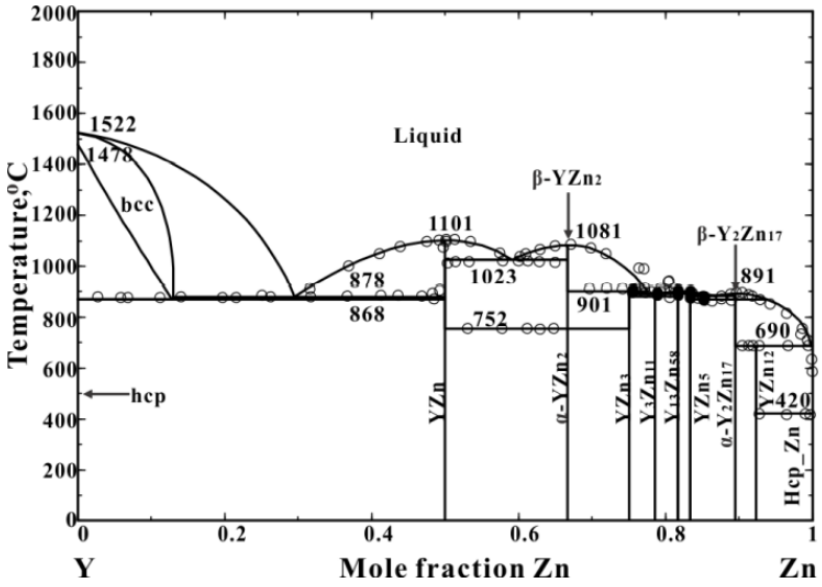

Figure 1. Yttrium–zinc phase diagram [109].

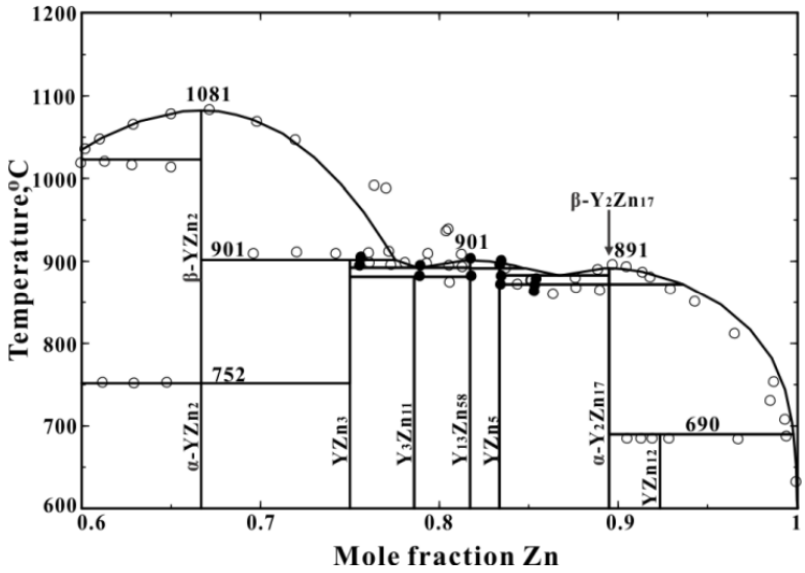

Figure 2. Yttrium–zinc phase diagram in Zn-rich region [109].

3. Zinc–Cerium Phase Diagram

The first Zn-Ce phase diagram was published by Hansen and Anderko [110]. Subsequently, Veleckis et al. [111] reported eight intermediate phases; $CeZn_{11}$, Ce_2Zn_{17}, CeZn, $CeZn_{8.8\text{-}6.2}$, $CeZn_2$, $CeZn_7$, Ce_2Zn, and Ce_4Zn. Okamoto and Hiroaki [112] suggested the existence of nine intermediate phases, namely CeZn, $CeZn_2$, $CeZn_3$, $CeZn_{3.67}$, $CeZn_{4.5}$, $CeZn_{5.25}$, $CeZn_7$, Ce_2Zn_{17}, and $CeZn_{11}$. The discrepancies in the stoichiometry and phase boundary reported by [110–112] were because of the delayed nucleation of these phases. Investigating the phase boundary and similarity of the Zn-Ce system to another Zn-RE phase diagram (such as Zn-Pr, Zn-Nd, Zn-Y, and Zn-Pm), nine intermetallic compounds were suggested [101,112–114]: CeZn, $CeZn_2$, $CeZn_3$, Ce_3Zn_{11}, $Ce_{13}Zn_{58}$, $CeZn_5$, Ce_3Zn_{22}, Ce_2Zn_{17}, and $CeZn_{11}$. A detailed investigation on the crystallographic data of intermetallic phases was presented in [114]. These intermediate compounds were included in the thermodynamic modeling of Zn-Ce phase diagram in the work of Wang et al. [115], Spencer et al. [98], and Zhu and Pelton [109]. The work of Chiotti and Mason [116] was the only experimental phase diagram data that could be found in the literature. Chiotti and Mason [116] inves-

tigated Zn-Ce phase diagram using metallography, differential thermal analysis (DTA), X-ray diffraction, and vapor pressure measurements. Johnson and Yonco [117] reported the standard Gibbs free energy of formation of the $CeZn_{11}$ phase, which was in accord with [116]. Chiotti and Mason [116] used dewpoint method to derive standard Gibbs free energy of formation for the intermetallic compounds. Johnson and Yonco [118] used the equation of standard Gibbs free energy to derive enthalpy of formation of the intermediate compounds.

Spencer et al. [98] and Zhu and Pelton [109] used modified quasi-chemical model to optimize liquid phase. Zn-Ce phase diagram published by [109] was an improvement to the work of Zhu and Pelton [109]. Zn-Ce phase diagram presented by Zhu and Pelton [109] is shown in Figure 3.

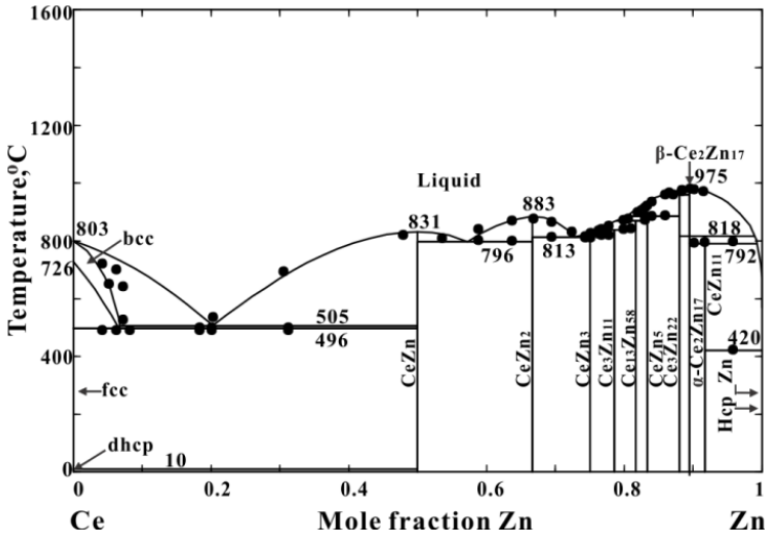

Figure 3. Zinc–cerium phase diagram calculated by [109].

4. Mg-Zn, Mg-Y, and Mg-Ce Phase Diagrams

Based on the literature, many researchers modeled liquid phase using a random solution model. This model is only anticipated at a very high temperature when the entropy term overwhelms any tendency for ordering or clustering of atoms. Therefore, the configurational entropy of mixing should vary with temperature. The modified quasi-chemical solution model has a better treatment of configurational entropy that accounts for a non-random distribution of atoms. Therefore, no model based on the random mixing can properly describe the influence of short-range ordering, because they do not solve the problem of the configurational entropy. The description of short-range ordering can be taken into account with bond energy models by considering the interactions between atoms that extend beyond the nearest neighbor's approximation. This problem has been treated using the modified quasi-chemical model. Liquid phase in the work of [77] was optimized using the modified quasi-chemical model (MQM). This model has been used to describe the liquid phase as this is the only scientific model that accounts for the presence of short-range ordering. Therefore, the reported phase diagrams in the work of [77] adequately describe thermodynamic properties of these systems. Islam et al. [77] critically reviewed and assessed thermodynamic data and phase diagrams of Mg-Zn, Mg-Y, and Mg-Ce systems. Figures 4–6 presented the most accurate calculated binary phase diagrams for these systems [77]. It is worth mentioning that the liquid phase was optimized using a modified quasi-chemical model to accurately describe short range ordering in the liquid.

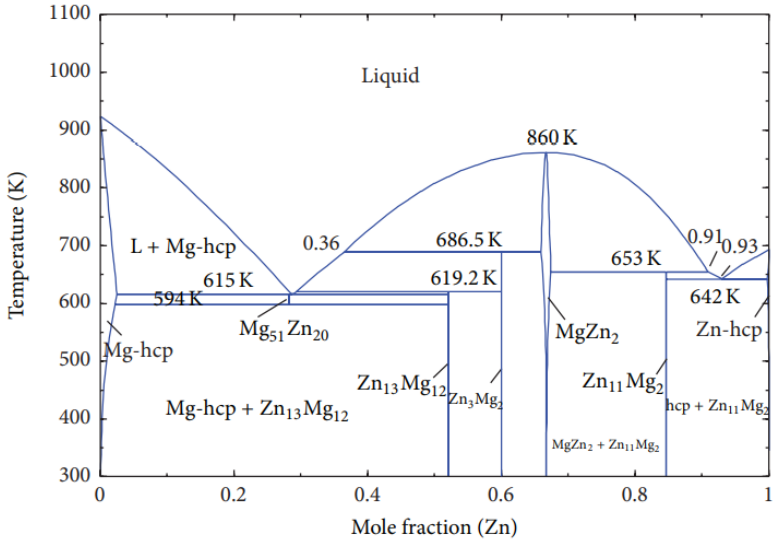

Figure 4. Mg-Zn phase diagram [119].

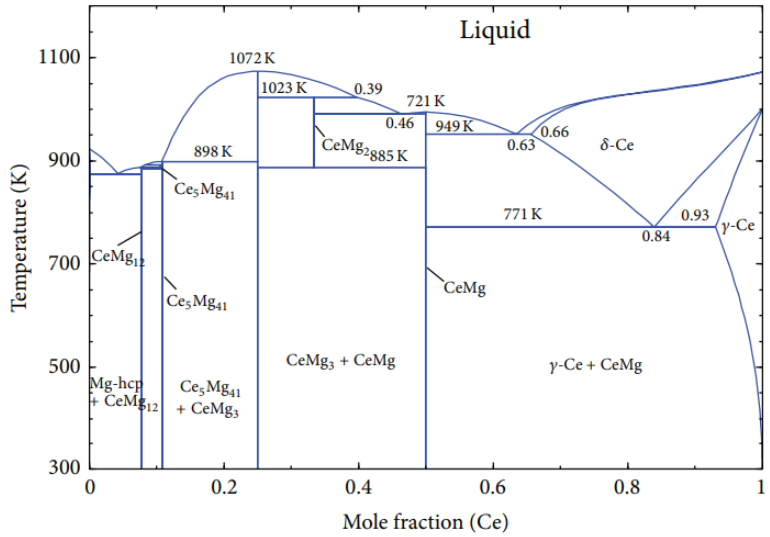

Figure 5. Mg-Ce phase diagram [77].

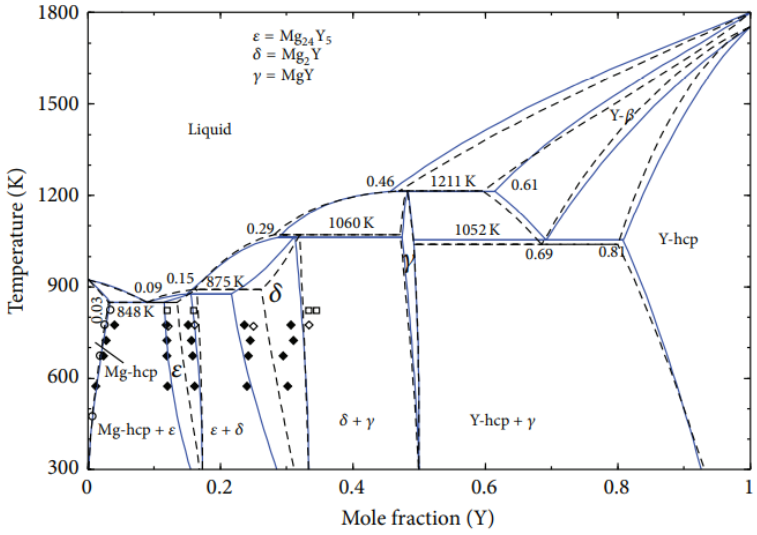

Figure 6. Mg-Y phase diagram solid lines [97] in comparison to [120] showed in dotted line [77].

5. Magnesium-Zinc-Yttrium Ternary Phase Diagram

Gröbner et al. [121] investigated the Mg-Zn-Y ternary system using ten ternary alloys by DSC, SEM/EDXS, and TEM. Based on their experimental results and assessment to the stoichiometric of ternary phases reported in the literature [96,122–140], Gröbner et al. [121] calculated liquidus projections and isothermal sections at 400, 500, and 600 °C. In 2015, Zhu and Pelton [140] calculated liquidus projection and isothermal sections at 400, 500, and 600 °C. Zhu and Pelton [140] defined ternary phase diagrams of Mg-Zn-RE systems using the Kohler model to estimate ternary properties of Mg-Zn-RE systems. It is worth mentioning that liquidus projections of Zhu and Pelton [140] and Gröbner et al. [121] are the only works that could be found in the literature. Gröbner et al. [121] modelled five ternary compounds: 18R, 14H, W, I, and Z, and one ternary solid solution (H). However, Zhu and Pelton [140] reported four ternary compounds (τ_5, H, X, and I phases) and three ternary solid solutions (Y(Mg,Zn), $Y_2(Mg,Zn)_{17}$, and τ_3 ($YMg(Mg,Zn)_2$).

Chemical compositions and notations of the ternary phases were confusing as described in the literature [96,121–140]. Many of the ternary phases reported in the literature were considered as metastable phases according to the work of Zhu and Pelton [140]. The slow kinetics of transformation of ternary phase, long-period stacking ordered (LPSO), has been described in the literature with different notations and chemical compositions [32–36,39,40,52,67,69,70,112,126,127,138]. This ternary phase exists in many Mg-Zn-RE systems which corresponds to $Mg_{12}ZnY_2$ [40,140] and was designated in the literature as X-phase with simplified composition $Mg_{12}YZn$ [96,127,140]. Ternary phase with notation of I-phase was reported by Tsai et al. [124] as $Mg_{30}Zn_{60}Y_{10}$ and later simplified as Mg_3Zn_6Y [138] and adopted in thermodynamic modeling in the work of [96,121,140]. Moreover, W-phase was reported in the work of [96] with composition of $Mg_3Zn_3Y_2$ and $Mg_{25}Zn_{60}Y_{14}$ [128], while Zhu and Pelton [140] and Gröbner et al. [121] described this phase as a ternary solid solution of yttrium in (MgZn) binary phase where yttrium may substitute magnesium and zinc element in the sublattice. Ternary phase designated as H-phase and composition of $Mg_{15}Zn_{70}Y_{15}$ [124] was accepted in the work of Zhu and Pelton [140]. Similarly to other Mg-Zn-RE ternary systems, this phase has been modeled as stoichiometric ternary compound. However, Gröbner et al. [121] describe this phase as ternary solid solubility of Mg in (YZn_5): $Y(Mg, Zn)_{1.5}Zn_{3.5}$ using the experimental data of [138]. Zhu and Pelton [140] treated H-phase differently because the crystallographic data (lattice constants) significantly differ from those of YZn_5 phase. Ternary solid solubility of Mg in $Zn_{17}Y_2$ binary phase, reported in the work of Zhu and Pelton- [140], was not observed in the liquidus projections of Gröbner et al. [121]. Based on the above confusion of the chemistry of ternary compounds, as well as ternary solid solutions in the Mg-Y-Zn system, further experimental investigation is required to resolve the discrepancies in the literature. Liquidus projections of the ternary Mg-Zn-Y phase diagram reported by Gröbner et al. [121] and Zhu and Pelton [140] are shown in Figure 7a,b, respectively.

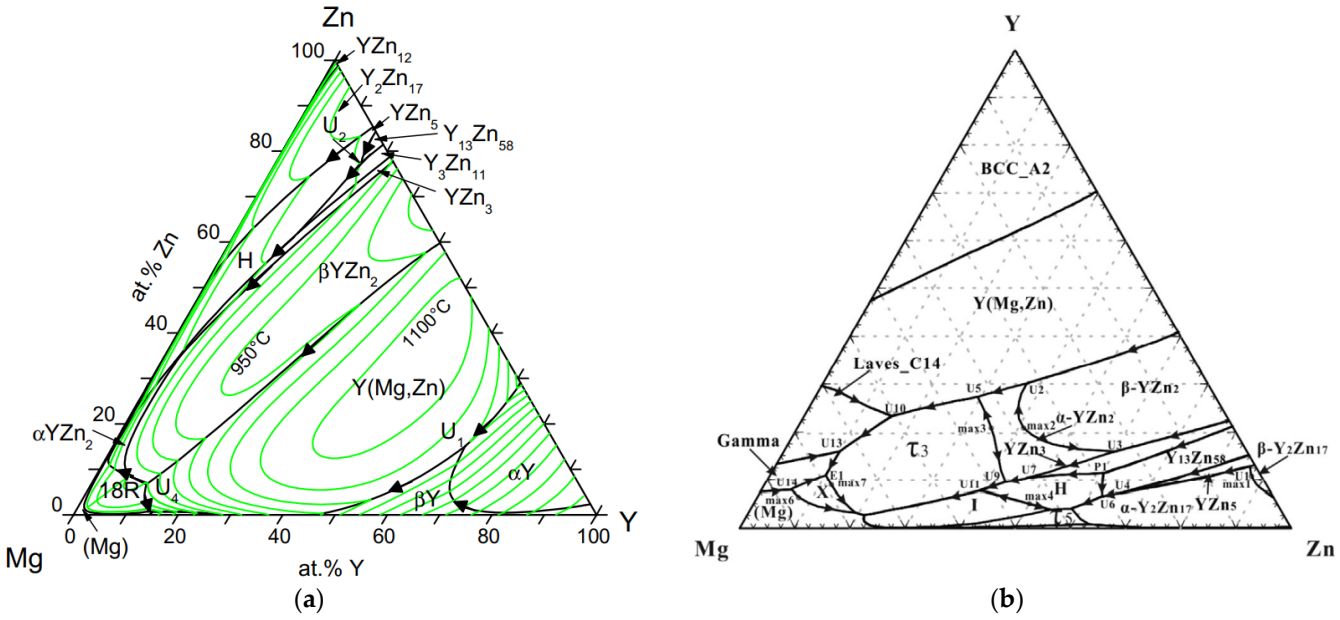

Figure 7. Liquidus projections of the ternary Mg-Zn-Y phase diagram; (**a**) Gröbner et al. [121] and (**b**) Zhu and Pelton [140].

6. Magnesium–Zinc–Cerium Ternary Phase Diagram

Experimental investigation and thermodynamic modeling of the Mg-Zn-Ce received considerable attention by many researchers [141–153]. However, the reported ternary phases and ternary solid solutions were confusing. Table 1 summarizes the reported ternary phases in the Mg-Zn-Ce system [151].

Table 1. Reported ternary phases in the Mg-Zn-Ce system in comparison with literature.

Phase	[149]	[151]	[150]	[146]	[145]	[144]
$Mg_{11}Zn_{83}Ce_6$	$Ce(Mg_{1-x}Zn_x)_{11}$	$Ce(Mg_{1-y}Zn_y)_{11}$	$Ce(Mg_{0.14}Zn_{0.86})_{11}$		$Ce(Mg_xZn_{1-x})_{10.1}$	
(Mg,Zn)Ce	(Mg,Zn)Ce	$MgZn_4Ce$	$Mg_{19}Zn_{81}$ Ce_{20}			
$(Mg,Zn150)_3Ce$	$(Mg,Zn)_3Ce$	$Mg_{2.3-x}Zn_{12.8+x}Ce$	Mg_xZn_yCe 1.2 x 2.3 12.8 y 13.9			$(Mg,Zn)_3Ce$
$Mg_{13}Zn_{30}Ce_3$	$Mg_7Zn_{12}Ce$	$Mg_7Zn_{12}Ce$			$Mg_7Zn_{12}Ce$	$Mg_7Zn_{12}Ce$
$Mg_5Zn_9Ce_2$	Mg_3Zn_5Ce	Mg_3Zn_5Ce	$Mg_{2.5}Zn_{4.5}Ce$			Mg_3Zn_5Ce
$Mg_{12}Ce$	$(Mg,Zn)_{12}Ce$	$Mg_3Zn_3Ce_2$	$Mg_{1+x}Zn_{2-x}Ce$	$Ce_{6.21}Mg_xZn_y$ 7.52 x 14.56 79.23 y 86.27		$Ce(Mg_xZn_{1-x})_9$
$Mg_{53}Zn_{45}Ce_2$	$Mg_{53}Zn_{45}Ce_2$	$Mg_{29}Zn_{25}Ce$	$Mg_{29.2}Zn_{24.8}Ce$	$Mg_{53.14}Zn_{45.04}Ce_{1.82}$		
$(Mg,Zn)_2Zn_9Ce_3$	$MgZn_2Ce$	$Mg_3Zn_{19}Ce_6$	$Mg_{13}Zn_{30}Ce_3$			
$Mg_{19}Zn_{81}Ce_{20}$						
Mg_3Ce	$(Mg,Zn)_2Ce$					

Ternary solid solution designated by Mg_3Ce was reported by [149,152] where zinc atom substitutes magnesium atom in the binary Mg_3Ce phase. The solubility of zinc in Mg_3Ce and crystallographic data are shown in Table 2. Recently, this phase was verified in the work of Shi et al. [153].

Table 2. Crystallographic data and Zn solubility in Mg_3Ce.

Phase Name	Pearson Symbol-Space Group	Zinc Solubility	Reference
Mg_3Ce	$cF16 - Fm\bar{3}m$	28 at.% at 300 °C	[149]
		28.4 at.% at 300 °C	[151]
		30 at.% at 300 °C	[144]
		36 at.% at 350 °C	[146]
		40 at.% at 197 °C	[150]
		6.4 at.% at 350 °C	[153]

Ternary solid solution, denoted as τ_3 in the work of [152,153], was reported by [144,150] with a prototype of $AlMnCu_2$. The percentage of zinc in this phase was 38 to 50 at.% [150], whereas Kevorkov and Pekguleryuz [148] reported this percentage as 45 to 50 at.%. Moreover, Mel'nik et al. [144] and Chiu et al. [149] reported that this phase contained 35 to 45, and 0 to 48 at.% Zn, respectively. It is worth noting that Chiu et al. [149] reported Mg_3Ce solid solution with two different prototypes, namely BiF_3 and $AlMnCu_2$. Whereas Shi et al. [153] verified the existence of τ_3 and indicated the difficulty to distinguish between τ_3 and Mg_3Ce because of the structural similarity. The authors of [153] declared the difficulty of detecting the difference using XRD. According to the BSE image in the work of [153], Mg_3Ce showed diamond shape whereas τ_3 exhibited irregular shape. Meanwhile, τ_3 exists in equilibrium with Mg_3Ce in accord with [152,153]. Reported comparisons between the crystallographic data and solid solubility for other ternary phases were summarized in the work of Chiu et al. [149] and Zhu et al. [152].

Liquidus projections of the Mg-Zn-Ce ternary phase diagram were calculated by [148–153]. The calculated ternary phase diagram by Chiu et al. [149] proposed that τ_3 and Mg_3Ce were similar phase, which contradicts the findings in [152,153]. Moreover, ternary phase diagram presented by Zhu et al. [152] was an amendment to the work of Mostafa and Medraj [151]. Primary crystallization regions of ternary phases could not be found in the liquidus projection of Shi et al. [153]. Liquidus projections of Mg-Zn-Ce calculated by Zhu et al. [152] and Shi et al. [153] are shown in Figure 8a,b, respectively.

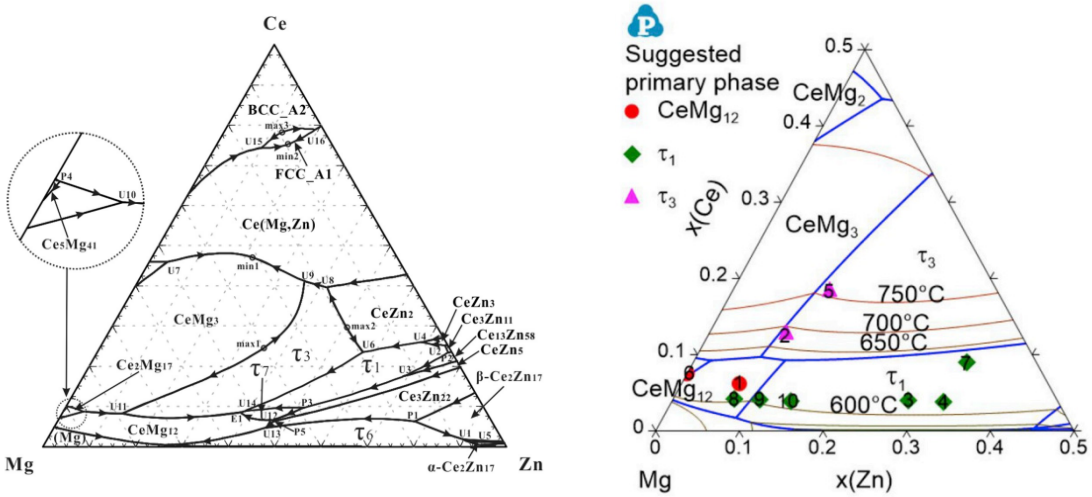

(**a**) (**b**)

Figure 8. Calculated liquidus projections of Mg-Zn-Ce presented in (**a**) Zhu et al. [152] and (**b**) Shi et al. [153].

7. Mechanical Properties of Mg-Zn-{Ce, Y} Alloys

Alloying Mg-Zn with rare earth elements is promising in modifying magnesium texture. Among rare-earth element, many researchers reported that micro-alloying Mg-Zn with yttrium or cerium exhibited a comparable ductility and formability with commercial magnesium alloys. Tables 3 and 4 summarize the mechanical properties of the published alloys in Mg-Zn-Y [154–157] and Mg-Zn-Ce [48,71,81,85,156–158], respectively.

Table 3. Mechanical properties of Mg-Zn-Y alloys.

Nominal Composition (wt.%)	Yield Strength (MPa)	Ultimate Tensile Strength (MPa)	Ductility	Process Conditions
Mg-2Zn+0.4Y	160	240	30%	Samples were cast at 690 °C and then extruded at 310 °C [154]
Mg-14.4Zn-3.3Y	365 ± 3.5	380	8%	Samples were cast and solutionized at 480 °C for 24 h followed by extrusion at 430 °C, then aged at 150 °C [155]
Mg-14.4Zn-3.3Y	171	320	12	Samples were cast and solutionized at 480 °C for 24 h followed by extrusion at 430 °C [155]
Mg-1.5Zn-0.2Y	135	238	17%	The ingots were homogenized at 450 °C for 12 h, then rolled at 400 °C, and after that sheet annealed at 350 °C for 1 h [156]
Mg-6.0Zn-1.0Y	268.3		12.9%	Alloys were solutionized at 480 °C and then extruded at 390 °C [157]
Mg-6.0Zn-1.0Y	288.7		17.3%	Alloys were solutionized at 480 °C and then extruded at 390 °C and aged at 150 °C for 48h [157]
Mg-3.0Zn-0.5Y	262	18.3%		Alloys were solutionized at 480 °C and then extruded at 350 °C [157]

Table 4. Mechanical properties of Mg-Zn-Ce alloys.

Nominal Composition (wt.%)	Yield Strength (MPa)	Ultimate Tensile Strength (MPa)	Ductility	Process Conditions
Mg-2Zn+0.4Ce	190	255	18%	Samples were cast at 690 °C and then extruded at 310 °C [48]
Mg-2Zn-0.2Ce (ZE20)	69	170	31%	Samples were cast at 700 °C and then extruded at 400 °C [48]
Mg-5Zn-0.2Ce (ZE50)	135	247	15%	
Mg-8Zn-0.2Ce (ZE80)	136	289	16%	

Table 4. *Cont.*

Nominal Composition (wt.%)	Yield Strength (MPa)	Ultimate Tensile Strength (MPa)	Ductility	Process Conditions
Mg-1.5Zn-0.2Ce	140	240	19%	The ingots were homogenized at 450 °C for 12h, then rolled at 400 °C and after that sheet annealed at 350° C for 1 h [156]
Mg-6Zn-0.2Ce	225	270	30%	Alloys were cast at 750 °C and homogenized at 350 °C for 12 h. After extrusion, alloys aged at 175 °C from 0.5 to 80 h [157]
Mg-2%Zn-0.5%Ce (ZE20)	199.2	~245	6%	Samples were prepared by continuous casting, then homogenized at 823 K for 8 h. Sheets were rolled by conventional rolling at 673 K [158]
Mg-2%Zn-0.5%Ce (ZE20)	125	~235	13.8%	Samples were prepared by continuous casting, then homogenized at 823 K for 8 h. Sheets were rolled by conventional rolling at 673 K. Sheets were annealed at 673 K [158]
Mg-2%Zn-0.5%Ce (ZE20)	~170	~240	28.23	Samples were prepared by continuous casting, then homogenized at 823 K for 8 h. Sheets were rolled by packed rolling at 673 K. Sheets were annealed at 673 K [158]
Mg-2%Zn-0.5%Ce (ZE20)	~165	~236	33.4%	Samples were prepared by continuous casting, then homogenized at 823 K for 8 h. Sheets were rolled by packed rolling at 723 K. Sheets were annealed at 723 K [158]
Mg-0.5Zn-0.2Ce	133	213	25%	Samples were heated at 723 K for 20 min and sheets were rolled by unidirectional rolling at 353 K. Then, sheets were annealed at 623 K for 90 min [81]
Mg-1.0Zn-0.2Ce	110	202	23%	
Mg-1.5Zn-0.2Ce	116	206	29%	
Mg-2.0Zn-0.2Ce	118	222	25%	
Mg-2.5Zn-0.2Ce	131	228	16%	
Mg-1.5Zn-0.2Ce	153	231	26%	Samples were extruded at 703 K and then annealed at 623K for 90 min [85]

Table 4. *Cont.*

Nominal Composition (wt.%)	Yield Strength (MPa)	Ultimate Tensile Strength (MPa)	Ductility	Process Conditions
Mg-1.5Zn-0.2Ce	194	248	20%	Samples were extruded at 573K and then annealed at 623K for 90 min [85]
Mg-1.0Zn-1.0Ce	95	191	22%	Samples were annealed at 350 °C and then annealed at 450 °C for 1 h [71]
Mg-2.0Zn-1.0Ce	101	197	26.2%	
Mg-4Zn-1.0Ce	109	220	18%	
Mg-1.0Zn-0.5Ce	95	191	30%	

The addition of yttrium to Mg-Zn alloys enhances the formation of magnesium solid solution in ternary systems due to high solid solubility of yttrium in magnesium. Meanwhile, precipitation of nano-scale ternary phases as a result enhances mechanical properties. It is worth noting that the ratio of Zn/Y and heat treatment conditions play a significant role in mechanical properties as can be seen in Table 3. Unlike yttrium, the micro-addition of cerium to Mg-Zn reduces magnesium solid solution and precipitates a binary Mg12Ce phase as well as ternary nano-scale phases. Maximum solid solubility of cerium in magnesium is 0.5 wt.% at 590 °C and Mg12Ce precipitate up to 32.4 wt.% Ce. The existence of cerium and zinc in magnesium resulted in weakening structure and therefore enhanced ductility of magnesium alloys. Meanwhile, the percentage of cerium magnesium alloys must be in small amounts to hinder precipitation of high intensity of Mg12Ce phase; besides, heat treatment conditions and weight fraction of cerium play a remarkable role in mechanical properties of Mg-Zn alloys as shown in Table 4.

8. Conclusions

To reduce oil consumption in the automobile industry, designers are interested in lightweight alternative materials. Among lightweight materials is magnesium, and products of Mg-Zn alloys used in the automobile industry include transmission housings, heads, and engine blocks. In the current work, thermodynamic modeling of yttrium-zinc and yttrium-cerium phase diagrams were critically assessed, and the most appropriate phase diagrams were presented. Crystallographic data and solid solubilities of ternary phases in Mg-Zn-Y and Mg-Zn-Ce systems were evaluated. Lack of experimental data on ternary Mg-Zn-Y required further experimental investigations. Based on the recent findings, liquidus projections of the Mg-Zn-Y and Mg-Zn-Ce ternary phase diagrams were given. Ternary intermetallic phases and ternary solid solution reported in the literature were confusing, and additional key experiments are needed to resolve the discrepancies on the existence and chemical compositions of these phases. Mechanical properties reported in the literature of the two ternary systems were summarized.

Author Contributions: Conceptualization, M.A. (Mohammad Aljarrah); methodology, M.A. (Mohammad Aljarrah), J.A. and M.A. (Mohammed Alhartomi).; software, M.A. (Mohammad Aljarrah); validation, M.A. (Mohammad Aljarrah), J.A. and M.A. (Mohammed Alhartomi); formal analysis, M.A. (Mohammad Aljarrah), J.A. and M.A. (Mohammed Alhartomi); investigation, M.A. (Mohammad Aljarrah); resources, M.A. (Mohammad Aljarrah), J.A. and M.A. (Mohammed Alhartomi); data curation, M.A. (Mohammad Aljarrah); writing—original draft preparation, M.A. (Mohammad Aljarrah), J.A. and M.A. (Mohammed Alhartomi); writing—review and editing, M.A. (Mohammad Aljarrah); visualization, J.A.; supervision, M.A. (Mohammad Aljarrah); project administration, M.A. (Mohammad Aljarrah). All authors have read and agreed to the published version of the manuscript.

Funding: This research received no external funding.

Data Availability Statement: Not applicable.

Conflicts of Interest: The authors declare no conflict of interest.

References

1. Mordike, B.L.; Ebert, T. Magnesium: Properties-applications-potential. *Mater. Sci. Eng. A* **2001**, *302*, 37–45. [CrossRef]
2. Luo, A.A.; Sachdev, A.K.; Powell, B.R. Advance casting technology for lightweight automotive applications. *China Foundry* **2010**, *7*, 463–469.
3. Pan, F.S.; Zhang, J.; Wang, J.F.; Yang, M.B.; Han, E.H.; Chen, R.S. Key R & D activities for development of new types of wrought magnesium alloys in China. *Trans. Nonferr. Met. Soc.* **2010**, *20*, 1249–1258.
4. Hong, Z.; Wei, L.; Xing, W.M.; Yu, Z. Study on ignition proof AZ91D magnesium alloy chips with cerium addition. *J. Rare Earths* **2005**, *23*, 466–469.
5. Wang, R.; Eliezer, A.; Gutman, E. An investigation on the microstructure of an AM50 magnesium alloy. *Mater. Sci. Eng. A* **2003**, *355*, 201–207. [CrossRef]
6. Kiani, M.; Gandikota, I.; Rohano, M.R.; Motoyama, K. Design of lightweight magnesium car body structure under crash and vibration constraints. *J. Magnes. Alloy* **2014**, *2*, 99–108. [CrossRef]
7. Wen, K.; Liu, K.; Wang, Z.; Li, S.; Du, W. Effect of microstructure evaluation on mechanical property of extruded Mg-$_{12}$Gd-$_{2}$Er-$_{1}$Xn-$_{0.6}$ Zr alloys. *J. Magnes. Alloy* **2015**, *3*, 23–28. [CrossRef]
8. Barnett, M.R.; Nave, M.D.; Bettles, C.J. Deformation microstructures and textures of some cold rolled mg alloys. *Mater. Sci. Eng. A* **2004**, *386*, 205–211. [CrossRef]
9. Stanford, N.; Atwell, D.; Beer, A.; Davies, C.; Barnett, M.R. Effect of microalloying with rare-earth elements on the texture of extruded magnesium-based alloys. *Scr. Mater.* **2008**, *59*, 772–775. [CrossRef]
10. Zhang, H.; Huang, G.; Wang, L.; Roven, H.J.; Xu, Z.; Pan, F. Improved ductility of magnesium alloys by a simple shear process followed by annealing. *Scr. Mater.* **2013**, *69*, 49–52. [CrossRef]
11. Sakamoto, M.; Akiyama, S.; Ogi, K. Suppression of Ignition and Burning of Molten Mg Alloys by Ca Bearing Stable Oxide Film. *J. Mater. Sci. Lett.* **1997**, *16*, 1048–1050. [CrossRef]
12. Stanford, N. The Effect of Calcium on the Texture, and Mechanical Properties of Extruded Mg–Mn–Ca Alloys. *Mater. Sci. Eng. A* **2010**, *528*, 314–322. [CrossRef]
13. Jing, B.; Yangshan, S.; Shan, X.; Feng, X.; Tianbai, Z. Microstructure and Tensile Creep Behavior of Mg–4Al Based Magnesium Alloys with Alkaline-Earth Elements Sr and Ca Additions. *Mater. Sci. Eng. A* **2006**, *419*, 181–188. [CrossRef]
14. Yoo, M.H. Slip, twinning, and fracture in hexagonal close-packed metals. *Metall. Trans. A* **1981**, *12*, 409–418. [CrossRef]
15. Tu, T.; Chen, X.; Zhao, C.; Yuan, Y.; Pan, F. A simultaneous increase of elastic modulus and ductility by Al and Li additions in Mg-Gd-Zn-Zr-Ag alloy. *Mater. Sci. Eng. A* **2020**, *771*, 138576. [CrossRef]
16. Zhang, A.; Kang, R.; Wu, L.; Pan, H.; Xie, H.; Huang, Q.; Liu, Y.; Ai, Z.; Ma, L.; Ren, Y.; et al. A new rare-earth-free Mg-Sn-Ca-Mn wrought alloy with ultra-high strength and good ductility. *Mater. Sci. Eng. A* **2019**, *754*, 269–274. [CrossRef]
17. Shin, D.H.; Kim, I.; Kim, J.; Kim, Y.S.; Semiatin, S.L. Microstructure development during equal-channel angular pressing of titanium. *Acta Mater.* **2003**, *51*, 983–996. [CrossRef]
18. Sun, H.Q.; Shi, Y.N.; Zhang, M.X.; Lu, K. Plastic strain-induced grain refinement in the nanometer scale in a Mg alloy. *Acta Mater.* **2007**, *55*, 975–982. [CrossRef]
19. Robson, J.D.; Henry, D.T.; Davis, B. Particle effects on recrystallization in magnesium–manganese alloys: Particle-stimulated nucleation. *Acta Mater.* **2009**, *2009*, 2739–2747. [CrossRef]
20. Karakulak, E. A review: Past, present, and future of grain refining of magnesium castings. *J. Magnes. Alloy.* **2019**, *7*, 355–369. [CrossRef]
21. Zhao, D.; Chen, X.; Ye, J.; Chen, T.; Dai, Y.; Liu, C.; Luo, Z.; Gao, S.; Zhang, J.; Yao, J.; et al. Simultaneously improving elastic modulus and damping capacity of extruded Mg-Gd-Y-Zn-Mn alloy via alloying with Si. *J. Alloys Compd.* **2019**, *810*, 425–435. [CrossRef]
22. Shen, Y.F.; Guan, R.G.; Zhao, Z.Y.; Misra, R.D.K. Ultrafine-grained Al–$_{0.2}$Sc–$_{0.1}$Zr alloy: The mechanistic contribution of nano-sized precipitates on grain refinement during the novel process of accumulative continuous extrusion. *Acta Mater.* **2015**, *100*, 247–255. [CrossRef]
23. Chen, Y.; Yang, Y.; Feng, Z.; Zhao, G.; Huang, B.; Luo, X.; Zhang, Y.; Zhang, W. Microstructure, microtexture and precipitation in the ultrafine-grained surface layer of an Al-Zn-Mg-Cu alloy processed by sliding friction treatment. *Mater. Charact.* **2017**, *123*, 1890197. [CrossRef]
24. Fu, L.; Li, Y.; Jiang, F.; Huang, J.; Xu, G.; Yin, Z. On the role of Sc or Er micro-alloying in the microstructure evolution of Al-Mg alloy sheets during annealing. *Mater. Charact.* **2019**, *157*, 109918. [CrossRef]
25. Lim, T.S.; Ryu, H.S.; Hong, S.-H. Plasma electrolytic oxidation/cerium conversion composite coatings for the improved corrosion protection of AZ31 Mg alloys. *J. Electrochem. Soc.* **2012**, *160*, C77.
26. Castellanos, A.; Altube, A.; Vega, J.M.; García-Lecina, E.; Díez, J.A.; Grande, H.J. Effect of different post-treatments on the corrosion resistance and tribological properties of AZ91D magnesium alloy coated PEO. *Surf. Coat. Tech.* **2015**, *278*, 99–107. [CrossRef]
27. Pérez, P.; Cabeza, S.; Garcés, G.; Adeva, P. Influence of long period stacking ordered phase arrangements on the corrosion behaviour of extruded $Mg_{97}Y_2Zn_1$ alloy. *Corros. Sci.* **2016**, *107*, 107–112. [CrossRef]
28. Lapovok, R.; Gao, X.; Nie, J.-F.; Estrin, Y.; Mathaudhu, S.N. Enhancement of properties in cast Mg–Y–Zn rod processed by severe plastic deformation. *Mater. Sci. Eng. A* **2014**, *615*, 198–207. [CrossRef]

29. Liu, C.; Chen, X.; Zhang, W.; Zhang, Y.; Pan, F. Microstructure, creep behavior and corrosion resistance in the ultrafine-grained surface layer of Mg-6Zn-0.2Y-0.4Ce-0.5Zr alloy processed by surfacing friction treatment. *Mater. Sci. Eng. A* **2020**, *776*, 138995. [CrossRef]
30. Laleh, M.; Kargar, F.; Rouhaghdam, A.S. Investigation of rare earth sealing of porous micro-arc oxidation coating formed on AZ91D magnesium alloy. *J. Rare Earths* **2012**, *30*, 1293–1297. [CrossRef]
31. Chen, B.; Lin, D.; Zeng, X.; Lu, C. Effects of yttrium and zinc addition on the microstructure and mechanical properties of Mg–Y–Zn alloys. *J. Mater. Sci.* **2010**, *45*, 2510–2517. [CrossRef]
32. Yamasaki, M.; Matsushita, M.; Hagihara, K.; Izuno, H.; Abe, E.; Kawamura, Y. Highly ordered 10H-type long-period stacking order phase in a Mg–Zn–Y ternary alloy. *Scr. Mater.* **2014**, *78–79*, 13–16. [CrossRef]
33. Lyu, J.; Kim, J.; Liao, H.; She, J.; Song, J.; Peng, J.; Pan, F.; Jiang, B. Effect of substitution of Zn with Ni on microstructure evolution and mechanical properties of LPSO dominant Mg–Y–Zn alloys. *Mater. Sci. Eng. A* **2020**, *773*, 138735. [CrossRef]
34. Hagihara, K.; Kinoshita, A.; Sugino, Y.; Yamasaki, M.; Kawamura, Y.; Yasuda, H.Y.; Umakoshi, Y. Effect of long-period stacking ordered phase on mechanical properties of $Mg_{97}Zn_1Y_2$ extruded alloy. *Acta Mater.* **2010**, *58*, 6282–6293. [CrossRef]
35. Tong, L.B.; Li, X.H.; Zhang, H.J. Effect of long period stacking ordered phase on the microstructure, texture, and mechanical properties of extruded Mg–Y–Zn alloy. *Mater. Sci. Eng. A* **2013**, *563*, 177–183. [CrossRef]
36. Zhu, S.M.; Lapovok, R.; Nie, J.F.; Estrin, Y.; Mathaudhu, S.N. Microstructure and mechanical properties of LPSO phase dominant $Mg_{85.8}Y_{7.1}Zn_{7.1}$ and $Mg_{85.8}Y_{7.1}Ni_{7.1}$ alloys. *Mater. Sci. Eng. A* **2017**, *692*, 35–42. [CrossRef]
37. Victoria-Hernández, J.; Yi, S.; Klaumünzer, D.; Letzig, D. Recrystallization behavior and its relationship with deformation mechanisms of a hot rolled Mg-Zn-Ca-Zr alloy. *Mater. Sci. Eng. A* **2019**, *761*, 138054. [CrossRef]
38. Zhang, W.; Wei, Q.; Huo, W.T.; Lu, J.W.; Hu, J.J.; Zhang, Y.S. Dynamic recrystallization in nanocrystalline AZ31 Mg-alloy. *Vacuum* **2017**, *143*, 236–240. [CrossRef]
39. Xu, D.; Han, E.; Xu, Y. Effect of long-period stacking ordered phase on microstructure, mechanical property, and corrosion resistance of Mg alloys: A review. *Proc. Natl. Sci.-Mater.* **2016**, *26*, 117–128. [CrossRef]
40. Kawamura, Y.; Yamasaki, M. Formation and mechanical properties of $Mg_{97}Zn_1RE_2$ alloys with long-period stacking ordered structure. *Mater. Trans.* **2007**, *48*, 2986–2992. [CrossRef]
41. Patel, V.; Li, W.; Liu, X.; Wen, Q.; Su, Y.; Shen, J.; Fu, B. Tailoring grain refinement through thickness in magnesium alloy via stationary shoulder friction stir processing and copper backing plate. *Mater. Sci. Eng. A* **2020**, *784*, 139322. [CrossRef]
42. Shahnam, A.; Karimzadeh, F.; Golozar, M.A.; Hosseini, S.N. Microstructure evolution of ultra-fine-grained AZ31 B magnesium alloy produced by submerged friction stir processing. *J. Mater. Eng. Perform.* **2019**, *28*, 4593–4601. [CrossRef]
43. Sun, W.T.; Qiao, X.G.; Zheng, M.Y.; Xu, C.; Kamado, S.; Zhao, X.J.; Chen, H.W.; Gao, N.; Starink, M.J. Altered ageing behaviour of a nanostructured $Mg_{-8.2}Gd_{-3.8}Y_{-1.0}Zn_{0.4}Zr$ alloy processed by high pressure torsion. *Acta Mater.* **2018**, *151*, 260–270. [CrossRef]
44. Yamasaki, M.; Hashimoto, K.; Hagihara, K.; Kawamura, Y. Effect of multimodal microstructure evolution on mechanical properties of Mg–Zn–Y extruded alloy. *Acta Mater.* **2011**, *59*, 3646–3658. [CrossRef]
45. Liu, H.; Ju, J.; Lu, F.; Yan, J.; Bai, J.; Jiang, J.; Ma, A. Dynamic precipitation behavior and mechanical property of an Mg94Y4Zn2 alloy prepared by multi-pass successive equal channel angular pressing. *Mater. Sci. Eng. A* **2017**, *682*, 255–259. [CrossRef]
46. Li, B.; Hou, X.; Teng, B. Effects of friction stir process and subsequent aging treatment on the microstructure evolution and mechanical properties of Mg-Gd-Y-Zn-Zr alloy. *Mater. Charact.* **2019**, *155*, 109832. [CrossRef]
47. Essadiqi, E.; Shehata, M.T.; Javaid, A.; Shen, G.; Aljarrah, M.; Verma, R.; Mishra, R. *Alloying and Process Design of Mg Sheet*; CANMET Materials: Ottawa, ON, Canada, 2011.
48. Jian, W.W.; Cheng, G.M.; Xu, W.Z.; Koch, C.C.; Wang, Q.D.; Zhu, Y.T.; Mathaudhu, S.N. Physics and model of strengthening by parallel stacking faults. *Appl. Phys. Lett.* **2013**, *103*, 133108. [CrossRef]
49. Shang, W.; Chen, B.; Shi, X.; Chen, Y.; Xiao, X. Electrochemical corrosion behavior of composite MAO/sol–gel coatings on magnesium alloy AZ91D using combined micro-arc oxidation and sol–gel technique. *J. Alloys Compd.* **2009**, *474*, 541–545. [CrossRef]
50. Zhang, Y.S.; Zhang, P.X.; Niu, H.Z.; Chen, C.; Wang, G.; Xiao, D.H.; Chen, X.H.; Yu, Z.T.; Yuan, S.B.; Bai, X.F. Surface nano-crystallization of Cu and Ta by sliding friction. *Mater. Sci. Eng. A* **2014**, *607*, 351–355. [CrossRef]
51. Zhang, W.; Lu, J.; Huo, W.; Zhang, Y.; Wei, Q. Microstructural evolution of AZ31 magnesium alloy subjected to sliding friction treatment. *Philos. Mag.* **2018**, *98*, 1576–1593. [CrossRef]
52. Jiang, M.G.; Xu, C.; Yan, H.; Fan, G.H.; Nakata, T.; Lao, C.S.; Chen, R.S.; Kamado, S.; Han, E.H.; Lu, B.H. Unveiling the formation of basal texture variations based on twinning and dynamic recrystallization in AZ31 magnesium alloy during extrusion. *Acta Mater.* **2018**, *157*, 53–71. [CrossRef]
53. González, S.; Pérez, P.; Garcés, G.; Adeva, P. Influence of the processing route on the mechanical properties at high temperatures of Mg-Ni-Y-RE alloys containing LPSO phases. *Mater. Sci. Eng. A* **2016**, *673*, 266–279. [CrossRef]
54. Li, X.; Liu, X.; Luan, B.L. Corrosion and wear properties of PEO coatings formed on AM60B alloy in $NaAlO_2$ electrolytes. *Appl. Surf. Sci.* **2011**, *257*, 9135–9141. [CrossRef]
55. Garces, G.; Muñoz-Morris, M.A.; Morris, D.G.; Perez, P.; Adeva, P. Optimization of strength by microstructural refinement of MgY_2Zn_1 alloy during extrusion and ECAP processing. *Mater. Sci. Eng. A* **2014**, *614*, 96–105. [CrossRef]
56. Aljarrah, M.; Essadiqi, E.; Kang, D.H.; Jung, I.H. Solidification microstructure and mechanical properties of hot rolled and annealed Mg sheet produced through twin roll casting route. *Mater. Sci. Forum* **2011**, *690*, 331–334. [CrossRef]

57. Huo, W.T.; Zhang, W.; Lu, J.W.; Zhang, Y.S. Simultaneously enhanced strength and corrosion resistance of Mg–$_3$Al–$_1$Zn alloy sheets with nano-grained surface layer produced by sliding friction treatment. *J. Alloys Compd.* **2017**, *720*, 324–331. [CrossRef]
58. Zhang, W.; Huo, W.T.; Lu, J.W.; Hu, J.J.; Wei, Q.; Zhang, Y.S. Gradient shear banding in a magnesium alloy induced by sliding friction treatment. *Vacuum* **2017**, *143*, 95–97. [CrossRef]
59. Zhao, C.; Li, Z.; Shi, J.; Chen, X.; Tu, T.; Luo, Z.; Cheng, R.; Atrens, A.; Pan, F. Strain hardening behavior of Mg–Y alloys after extrusion process. *J. Magnes. Alloy.* **2019**, *7*, 672–680. [CrossRef]
60. Zhao, D.; Chen, X.; Wang, X.; Pan, F. Effect of impurity reduction on dynamic recrystallization, texture evolution and mechanical anisotropy of rolled AZ31 alloy. *Mater. Sci. Eng. A* **2020**, *773*, 138741. [CrossRef]
61. Aljarrah, M.; Essadiqi, E. On the precipitates and mechanical properties of magnesium-yttrium sheets. *Alex. Eng. J.* **2013**, *52*, 221–225. [CrossRef]
62. Xu, S.W.; Zheng, M.Y.; Kamado, S.; Wu, K.; Wang, G.J.; Lv, X.Y. Dynamic microstructural changes during hot extrusion and mechanical properties of a Mg–$_{5.0}$ Zn–$_{0.9}$ Y–$_{0.16}$ Zr (wt.%) alloy. *Mater. Sci. Eng. A* **2011**, *528*, 4055–4067. [CrossRef]
63. Wang, C.; Liu, Y.; Lin, T.; Luo, T.; Zhao, Y.; Hou, H.; Yang, Y. Hot compression deformation behavior of Mg-$_5$Zn-$_{3.5}$Sn-$_1$Mn-$_{0.5}$Ca-$_{0.5}$Cu alloy. *Mater. Charact.* **2019**, *157*, 109896. [CrossRef]
64. Sitdikov, R.K.O. Dynamic recrystallization in pure magnesium. *Mater. Trans.* **2001**, *42*, 1928–1937. [CrossRef]
65. Chen, Y.; Yang, Y.; Feng, Z.; Huang, B.; Luo, X.; Zhang, W. The depth-dependent gradient deformation bands in a sliding friction treated Al-Zn-Mg-Cu alloy. *Mater. Charact.* **2017**, *132*, 269–279. [CrossRef]
66. Wei, Y.H.; Liu, B.S.; Hou, L.F.; Xu, B.S.; Liu, G. Characterization and properties of nanocrystalline surface layer in Mg alloy induced by surface mechanical attrition treatment. *J. Alloys Compd.* **2008**, *452*, 336–342. [CrossRef]
67. Woo, W.; Choo, H.; Brown, D.W.; Liaw, P.K.; Feng, Z. Texture variation and its influence on the tensile behavior of a friction-stir processed magnesium alloy. *Scr. Mater.* **2006**, *54*, 1859–1864. [CrossRef]
68. Nishioka, T.; Yamamoto, Y.; Kimura, K.; Hagihara, K.; Izuno, H.; Happo, N.; Hosokawa, S.; Abe, E.; Suzuki, M.; Matsushita, T.; et al. In-plane positional correlations among dopants in 10H type long period stacking ordered $Mg_{75}Zn_{10}Y_{15}$ alloy studied by X-ray fluorescence holography. *Materialia* **2018**, *3*, 256–259. [CrossRef]
69. Kawamura, Y.; Hayashi, K.; Inoue, A.; Masumoto, T. Rapidly solidified powder metallurgy $Mg_{97}Zn_1Y_2$ alloys with excellent tensile yield strength above 600 MPa. *Mater. Trans.* **2001**, *42*, 1172–1176. [CrossRef]
70. Zhang, J.; Xu, J.; Cheng, W.; Chen, C.; Kang, J. Corrosion behavior of Mg–Zn–Y alloy with long-period stacking ordered structures. *J. Mater. Sci. Tech.* **2012**, *28*, 1157–1162. [CrossRef]
71. Li, C.Q.; Xu, D.K.; Zeng, Z.R.; Wang, B.J.; Sheng, L.Y.; Chen, X.B.; Han, E.H. Effect of volume fraction of LPSO phases on corrosion and mechanical properties of Mg-Zn-Y alloys. *Mater. Des.* **2017**, *121*, 430–441. [CrossRef]
72. Aljarrah, M.; Essadiqi, E.; Fouad, R.H.; Rababah, M.; Almagableh, A. The effect of annealing conditions and alloying elements on the microstructure stability and mechanical properties of Mg-Zn-Ce sheets. *Appl. Mech. Mater.* **2014**, *472*, 937–947. [CrossRef]
73. Liu, L.; Pan, F.; Chen, X.; Huang, Y.; Song, B.; Yang, H.; Hort, N. The effect of Y addition on recrystallization and mechanical properties of Mg–$_6$Zn–xY–$_{0.5}$Ce–$_{0.4}$Zr alloys. *Vacuum* **2018**, *155*, 445–455. [CrossRef]
74. Mingo, B.; Arrabal, R.; Mohedano, M.; Llamazares, Y.; Matykina, E.; Yerokhin, A.; Pardo, A. Influence of sealing post-treatments on the corrosion resistance of PEO coated AZ91 magnesium alloy. *Appl. Surf. Sci.* **2018**, *433*, 653–667. [CrossRef]
75. Jain, V.; Su, J.Q.; Mishra, R.S.; Verma, R.; Javaid, A.; Aljarrah, M.; Essadiqi, E. *Microstructure and Mechanical Properties of Mg-$_{1.7}$ Y-$_{1.2}$ Zn Sheet Processed by Hot Rolling and Friction Stir Processing*; Springer: Cham, Switzerland, 2011; pp. 565–570.
76. Liu, M.; Uggowitzer, P.J.; Nagasekhar, A.V.; Schmutz, P.; Easton, M.; Song, G.-L.; Atrens, A. Calculated phase diagrams and the corrosion of die-cast Mg–Al alloys. *Corros. Sci.* **2009**, *51*, 602–619. [CrossRef]
77. Wang, G.; Huang, G.; Chen, X.; Deng, Q.; Tang, A.; Jiang, B.; Pan, F. Effects of Zn addition on the mechanical properties and texture of extruded Mg-Zn-Ca-Ce magnesium alloy sheets. *Mater. Sci. Eng. A* **2017**, *705*, 46–54. [CrossRef]
78. Islam, M.M.; Mostafa, A.O.; Medraj, M. Essential magnesium alloys binary phase diagrams and their thermodynamic data. *J. Mater.* **2014**, *2014*, 704283.
79. Stanford, N.; Cottam, R.; Davis, B.; Robson, J. Evaluating the Effect of Yttrium as a Solute Strengthener in Magnesium Using in Situ Neutron Diffraction. *Acta Mater.* **2014**, *78*, 1–13. [CrossRef]
80. Gao, L.; Chen, R.S.; Han, E.H. Solid Solution Strengthening Behaviors in Binary Mg–Y Single Phase Alloys. *J. Alloys Compd.* **2009**, *472*, 234–240. [CrossRef]
81. Gao, L.; Chen, R.S.; Han, E.H. Effects of Rare-Earth Elements Gd and Y on the Solid Solution Strengthening of Mg Alloys. *J. Alloys Compd.* **2009**, *481*, 379–384. [CrossRef]
82. Chino, Y.; Huang, Z.; Suzuki, K.; Sassa, K.; Mabuchi, M. Influence of Zn concentration on stretch formability at room temperature of Mg-Zn-Ce alloy. *Mater. Sci. Eng. A* **2010**, *528*, 566–572. [CrossRef]
83. Zhou, T.; Xia, H.; Chen, Z.H. Effect of Ce on microstructures and mechanical properties of rapidly solidified Mg–Zn alloy. *Mater. Sci. Tech.* **2011**, *27*, 1198–1205. [CrossRef]
84. Langelier, B.; Esmaeili, S. Effects of Ce additions on the age hardening response of Mg–Zn alloys. *Mater. Charact.* **2015**, *101*, 1–8. [CrossRef]
85. Luo, A.A.; Mishra, R.K.; Sachdev, A.K. High-ductility magnesium-zinc-cerium extrusion alloys. *Scr. Mater.* **2011**, *64*, 410–413. [CrossRef]

86. Chino, Y.; Huang, X.; Suzuki1, K.; Sassa, K.; Mabuchi, M. Microstructure, Texture and Mechanical Properties of Mg-Zn-Ce Alloy Extruded at Different Temperatures. *Mater. Trans.* **2011**, *52*, 1104–1107. [CrossRef]
87. Mackenzie, L.W.F.; Pekguleryuz, M.O. The recrystallization and texture of magnesium-zinc-cerium alloys. *Scr. Mater.* **2008**, *59*, 665–668. [CrossRef]
88. Guo, X.; Remennik, S.; Xu, C.; Shechtman, D. Development of Mg-6.0%Zn-1.0%Y-0.6%Ce-0.6% Zr magnesium alloy and its microstructural evolution during processing. *Mater. Sci. Eng. A* **2008**, *473*, 266–273. [CrossRef]
89. Guo, X.; Kinstler, J.; Glazman, L.; Shechtman, D. High strength Mg-Zn-Y-Ce-Zr alloy bars prepared by RD and extrusion technology. *Mater. Sci. Forum* **2005**, *488–489*, 495–498. [CrossRef]
90. Kaufmann, L.; Bernstein, H. *Computer Calculation of Phase Diagrams with Special Reference to Refractory Metals*; Academic Press: Cambridge, MA, USA, 1970.
91. Lukas, H. *Computational Thermodynamics: The Calphad Method*; Cambridge University Press: Cambridge, UK, 2007.
92. Hillert, M. The compound energy formalism. *J. Alloys Compd.* **2001**, *320*, 161–176. [CrossRef]
93. Pelton, A.D.; Degterov, S.A.; Eriksson, G.; Robelin, C.; Dessureault, Y. The modified quasichemical model I—binary solutions. *Metall. Mater. Trans. B* **2000**, *31*, 651–659. [CrossRef]
94. Chiotti, P.; Mason, J.T.; Gill, K.J. Phase Diagram and Thermodynamic Properties of the Yttrium—Zinc System. *Trans. TMS-AIME* **1963**, *227*, 910–916.
95. Mason, J.T.; Chiotti, P. Phase diagram and thermodynamic properties of the yttrium-zinc system. *Metall. Trans. A* **1976**, *7*, 287–291. [CrossRef]
96. Shao, G.; Varsani, V.; Fan, Z. Thermodynamic modelling of the Y-Zn and Mg-Zn-Y systems. *Calphad* **2006**, *30*, 286–295, Erratum in *Calphad* **2007**, *31*, 313. [CrossRef]
97. Liu, X.J.; Wen, M.Z.; Wang, C.P.; Pan, F.S. Thermodynamic assessment of the Zn-Y and Al-Zn-Y systems. *J. Alloys Compd.* **2008**, *452*, 283–290. [CrossRef]
98. Spencer, P.J.; Pelton, A.D.; Kang, Y.B.; Chartrand, P.; Fuerst, C.D. Thermodynamic assessment of the Ca-Zn, Sr-Zn, Y-Zn and Ce-Zn systems. *Calphad* **2008**, *32*, 423–431. [CrossRef]
99. Harsha, K.S. The Crystal Structures of Intermetallic Compounds in the Yttrium-Zinc System. Ph.D. Thesis, Pennsylvania State University, State College, PA, USA, 1964.
100. Veleckis, E.; Schablaske, R.V.; Johnson, I.; Feder, H.M. Intermetallic phases in the systems of zinc with lanthanum, cerium, praseodymium, neodymium, and yttrium. *Trans. TMS-AIME* **1967**, *239*, 58.
101. Bruzzone, G.; Fornasini, M.L.; Merlo, F. Rare-earth intermediate phases with zinc. *J. Less-Common Met.* **1970**, *22*, 253–264. [CrossRef]
102. Fornasini, M.L. Crystal structnre of (Ho-, Er-, Tm-, Lu-, Y-) Zn, and $ThCd_5$ intermetallic compounds. *J. Less-Common Met.* **1971**, *25*, 329–333. [CrossRef]
103. Ryba, E. Transformation in AB2 Intermetallic Compounds, US Atomic Energy Comm. Report COO-3415-3. 1963. Available online: https://www.osti.gov/servlets/purl/4272069 (accessed on 7 December 2021).
104. Butorov, V.P.; Nichkov, I.F.; Novikov, E.A.; Raspopin, S.P. Izv. Vyssh. Ucheb. Zaved. *Tsvetn. Met.* **1973**, *15*, 96.
105. Hoshino, Y.; Plambeck, J.A. Electrochemical studies of yttrium and ytterium-zinc alloys in fused LiCl-KCl eutectic. *Can. J. Chem.* **1970**, *48*, 685–687. [CrossRef]
106. Yamschikov, L.F.; Lebedev, V.A.; Nichkov, N.F. Metally. *Izv. Akad. Nauk SSSR* **1979**, *83*.
107. Marquina, C.; Kim-Ngan, N.H.; Bakker, K.; Radwanski, R.J.; Jacobs, T.H.; Buschow, K.H.J.; Franse, J.J.M.; Ibarra, M.R. Specific heats of R_2Zn_{17} intermetallic compounds. *J. Phys. Condens. Matter.* **1993**, *5*, 2009. [CrossRef]
108. Morishita, M.; Yamamoto, H.; Tsuboki, K.; Horike, T. Standard Gibbs energy of formation of $Zn_{17}Y2$ and $Zn_{12}Y$ determined by solution calorimetry and measurement of heat capacity near zero kelvin. *Int. J. Mater. Res.* **2007**, *98*, 10–15. [CrossRef]
109. Zhu, Z.; Pelton, A.D. Critical assessment and optimization of phase diagrams and thermodynamic properties of RE–Zn systems—Part II—Y–Zn, Eu–Zn, Gd–Zn, Tb–Zn, Dy–Zn, Ho–Zn, Er–Zn, Tm–Zn, Yb–Zn and Lu–Zn. *J. Alloys Compd.* **2015**, *641*, 261–271. [CrossRef]
110. Hansen, M.; Anderko, K. *Constitution of Binary Alloys*, 2nd ed.; McGraw-Hill Book Go., Inc.: New York, NY, USA, 1958.
111. Veleckis, E.; Rosen, C.L.; Feder, H.M. A recording effusion balance for phase diagram investigation: U-Cd, U-Zn and Ce-Zn systems. *Phys. Chem.* **1961**, *65*, 2127–2131. [CrossRef]
112. Okamoto, H.; Hiroaki, T.B. *Binary Alloy Phase Diagrams*; ASM International, Materials Park: Geauga County, OH, USA, 1990.
113. Kripyakevich, P.I.; Kuz'ma, Y.B.; Ugrin, N.S. Crystal Structures of the compounds Ce3Zn22, La3Zn22, and Pr3Zn22. *J. Struct. Chem.* **1967**, *8*, 632–633. [CrossRef]
114. Malik, Z.P. On the Quaternary Systems Ce-Ni-Zn-{B, Si}. Ph.D. Thesis, University of Vienna, Vienna, Austria, 2012.
115. Wang, C.P.; Chen, X.; Liu, X.J.; Pan, F.S.; Ishida, K. Thermodynamic modeling of the Ce-Zn and Pr-Zn systems. *J. Alloys Compd.* **2008**, *458*, 166–173. [CrossRef]
116. Chiotti, P.; Mason, J.T. Phase relations and thermodynamic properties for the cerium-zinc systems. *Trans. AIME* **1965**, *233*, 786–795.
117. Johnson, I.; Yonco, R.M. *Atomic Energy Commission Research and Development Report ANL 6231*; Office of Technical Services, U.S. Department of Commerce: Washington, DC, USA, 1960; p. 78.

118. Johnson, I.; Yonco, R.M. Thermodynamics of Cadmium- and Zinc-Rich Alloys in the Cd-La, Cd-Ce, Cd-Pr, Zn-La, Zn-Ce and Zn-Pr Systems. *Met. Trans.* **1970**, *1*, 905–910.
119. Ghosh, P.; Mezbahul-Islam, M.; Medraj, M. Critical assessment and thermodynamic modeling of Mg-Zn, Mg-Sn, Sn-Zn and Mg-Sn-Zn systems. *Calphad* **2012**, *36*, 28–43. [CrossRef]
120. Islam, M.M.; Kevorkov, D.; Medraj, M. The equilibrium phase diagram of the magnesium-copper-yttrium system. *J. Chem. Thermodyn.* **2008**, *40*, 1064–1076. [CrossRef]
121. Gröbner, J.; Kozlov, A.; Fang, X.Y.; Geng, J.; Nie, J.F.; Schmid-Fetzer, R. Phase equilibria and transformations in ternary Mg-rich Mg-Y-Zn alloys. *Acta Mater.* **2012**, *60*, 5948–5962. [CrossRef]
122. Ping, D.H.; Hono, K.; Kawamura, Y.; Inoue, A. Local chemistry of a nanocrystalline high-strength $Mg_{97}Y_2Zn_1$ alloy. *Philos. Mag. Lett.* **2002**, *82*, 543–551. [CrossRef]
123. Villars, P.; Calvert, L.D. *Pearson's Handbook of Crystallographic Data for Intermetallic Phases*; ASM International, Materials Park: Geauga County, OH, USA, 1985.
124. Tsai, A.P.; Murakami, Y.; Niikura, A. The Zn-Mg-Y phase diagram involving quasicrystals. *Philos. Mag. A* **2000**, *80*, 1043–1054. [CrossRef]
125. Singh, A.; Watanabe, M.; Kato, A.; Tsai, A.P. Formation of icosahedral-hexagonal H phase nano-composites in Mg-Zn-Y alloys. *Scr. Mater.* **2004**, *51*, 955–960. [CrossRef]
126. Zhu, Y.M.; Morton, A.J.; Nie, J.F. The 18R and 14H long-period stacking ordered structures in Mg-Y-Zn alloys. *Acta Mater.* **2010**, *58*, 2936–2947. [CrossRef]
127. Pedezhnova, E.M.; Mel'nik, E.V.; Miliyevskiy, R.A.; Dobatkina, T.V.; Kinzhibalo, V.V. Investigation of the Mg-Zn-Y System. *Russ. Metall.* **1982**, *4*, 185–188.
128. Matsuda, M.; Ii, S.; Kawamura, Y.; Ikuhara, Y.; Nishida, M. Variation of long-period stacking order structures in rapidly solidified $Mg_{97}Zn_1Y_2$ alloy. *Mater. Sci. Eng. A* **2005**, *393*, 269–274. [CrossRef]
129. Deng, D.W.; Kuo, K.H.; Luo, Z.P.; Miller, D.J.; Kramer, M.J.; Dennis, K.W. Crystal structure of the hexagonal Zn_3MgY. *J. Alloys Compd.* **2004**, *373*, 156–160. [CrossRef]
130. Takakura, H.; Sato, A.; Yamamoto, A.; Tsai, A.P. Crystal structure of a hexagonal phase and its relation to a quasicrystalline phase in Zn-Mg-Y alloy. *Philos. Mag. Lett.* **1998**, *78*, 263–270. [CrossRef]
131. Luo, Z.P.; Zhang, S.Q. High-resolution electron microscopy on the X-$Mg_{12}ZnY$ phase in ahigh strength Mg-Zn-Zr-Y magnesium alloy. *J. Mater. Sci. Lett.* **2000**, *19*, 813–815. [CrossRef]
132. Luo, Z.P.; Zhang, S.; Tang, Y.; Zhao, D. Quasicrystals in as-cast Mg-Zn-RE alloys. *Scr. Metall. Mater.* **1993**, *28*, 1513–1518. [CrossRef]
133. Luo, Z.P.; Zhang, S.Q.; Tang, Y.L.; Zhao, D.S. On the stable quasicrystals in slowly cooled Mg-Zn-Y alloys. *Scr. Metall. Mater.* **1995**, *32*, 1411–1416. [CrossRef]
134. Luo, Z.P.; Sui, H.X.; Zhang, S.Q. On the stable Mg-Zn-Y quasicrystals. *Metall. Mater. Trans. A* **1996**, *27*, 1779–1784. [CrossRef]
135. Tsai, A.P.; Nijkura, A.; Inoue, A.; Masumoto, T. Stoichiometric icosahedral phase in the Zn-Mg-Y system. *J. Mater. Res.* **1997**, *12*, 1468–1471. [CrossRef]
136. Abe, E.; Takakura, H.; Singh, H.; Tsai, A.P. Hexagonal superstructures in the Zn-Mg-rare-earth alloys. *J. Alloys Compd.* **1999**, *283*, 169–172. [CrossRef]
137. Li, M.R.; Kuo, K.H. Intermetallic phases and phase reactions in Zn-Mg (<40 at.%)-Y (<20 at.%) region. *J. Alloys Compd.* **2007**, *432*, 81–89. [CrossRef]
138. Shao, G.; Varsani, V.; Wang, Y.; Qian, M.; Fan, Z. On the solidification microstructure of $Mg_{30}Zn_{2.5}Y$ metal-intermetallic alloy. *Intermetallics* **2006**, *14*, 596–602. [CrossRef]
139. Li, M.R.; Zou, X.D.; Kuo, K.H. Anew hexagonal phase displaying pseudo-icosahedral symmetry in Zn-Mg-Y alloy. *Scr. Mater.* **2009**, *60*, 683–686. [CrossRef]
140. Zhu, Z.; Pelton, A.D. Thermodynamic modeling of the Y-Mg-Zn, Gd-Mg-Zn, Tb-Mg-Zn, Dy-Mg-Zn, Ho-Mg-Zn, Er-Mg-Zn, Tm-Mg-Zn and Lu-Mg-Zn systems. *J. Alloys Compd.* **2015**, *652*, 426–443. [CrossRef]
141. Huang, M.; Li, H.; Ding, H.; Ren, Y.; Qin, G.; Hao, S. Partial phase relationships of Mg-Zn-Ce system at 350 °C. *Trans. Nonferr. Met. Soc.* **2009**, *19*, 681–685. [CrossRef]
142. Huang, M.; Li, H.; Ding, H.; Bao, L.; Ma, X.; Hao, S. Intermetallics and phase relations of Mg-Zn-Ce alloys at 400 °C. *Trans. Nonferr. Met. Soc.* **2012**, *22*, 539–545. [CrossRef]
143. Korolkov, A.M.; Saldau, Y.P. Solubility of Zn and Ce in Mg in the solid state. *Izv Sekt. Fiz-Khim Anal.* **1946**, *16*, 295–306.
144. Mel'nik, E.V.; Kostina, M.F.; Yarmlyuk, Y.P.; Zmii, O.F. Study of the magnesium-zinc-cerium and magnesium-zinc-calcium ternary systems. *Magnievye Splavy. Mater. Vses. Soveshch. Issled. Razrab. Primen. Magnievyhk Splavov* **1978**, *9599*.
145. Drits, M.E.; Drozdova, E.I.; Korolkova, I.G.; Kinzhibalo, V.V.; Tyvanchuk, A.T. Investigation of polythermal sections of the Mg-Zn-Ce system in the Mg-rich region. *Russ. Metall.* **1989**, *2*, 195–197.
146. Kolitsch, U.; Bellen, P.; Kaesche, S.; Maccio, D.; Bochvar, N.; Liberov, Y.; Rogl, P. Cerium-magnesium-zinc. In *Ternary Alloys—A Comprehensive Compendium of Evaluated Constitutional Data and Phase Diagrams*; Effenberg, G., Petzow, G., Eds.; VCH Verlagsgesellscahft, MSI GmbH: Stuttgart, Germany, 2000; pp. 168–176.
147. Agarwal, R.; Fries, S.G.; Lukas, H.L.; Petzow, G.; Sommer, F.; Chart, T.G.; Effenberg, G. Assessment of the Mg-Zn system. *Z. Für Metall.* **1992**, *83*, 216–223. [CrossRef]

148. Kevorkov, D.; Pekguleryuz, M. Experimental study of the Ce-Mg-Zn phase diagram at 350 °C via diffusion couple techniques. *J. Alloys Compnd.* **2009**, *478*, 427–436. [CrossRef]
149. Chiu, C.; Gröbner, J.; Kozlov, A.; Schmid-Fetzer, R. Experimental study and thermodynamic assessment of ternary Mg-Zn-Ce phase relations focused on Mg-rich region. *Intermetallics* **2010**, *18*, 399–405. [CrossRef]
150. Pavlyuk, V.; Marciniak, B.; Różycka, E.S. The isothermal section of the phase diagram of Ce–Mg–Zn ternary system at 470 K. *Intermetallics* **2012**, *20*, 8–15. [CrossRef]
151. Mostafa, A.; Medraj, M. Phase equilibria of the Ce-Mg-Zn ternary system at 300 °C. *Metals* **2014**, *4*, 168–195. [CrossRef]
152. Zhu, Z.; Gharghouri, M.A.; Medraj, M.; Lee, S.Y.; Pelton, A.D. Thermodynamic modelling and in-situ neutron diffraction investigation of the (Ce + Mg + Zn) system. *J. Chem. Thermodyn.* **2016**, *93*, 242–254. [CrossRef]
153. Shi, H.; Li, Q.; Zhang, J.; Luo, Q.; Chou, K. Re-assessment of the Mg-Zn-Ce system focusing on the phase equilibria in Mg-rich corner. *Calphad* **2020**, *68*, 101742. [CrossRef]
154. Le, Q.C.; Zhang, Z.Q.; Shao, Z.W.; Cui, J.Z.; Xie, Y. Microstructures and mechanical properties of Mg-2%Zn-0.4%Re alloys. *Trans. Nonferr. Met. Soc. China* **2010**, *20*, 352–356. [CrossRef]
155. Singh, A.; Somekawa, H.; Mukai, T. High temperature processing of Mg–Zn–Y alloys containing quasicrystal phase for high strength. *Mater. Sci. Eng. A* **2011**, *528*, 6647–6651. [CrossRef]
156. Liu, P.; Jiang, H.; Cai, Z.; Kang, Q.; Zhang, Y. The effect of Y, Ce and Gd on texture, recrystallization and mechanical property of Mg-Zn alloys. *J. Magnes.* **2016**, *4*, 188–196. [CrossRef]
157. Singh, A. Tailoring microstructure of Mg-Zn-Y alloys with quasicrystal and related phases for high mechanical strength. *Sci. Technol. Adv. Mater.* **2014**, *15*, 44803. [CrossRef]
158. Du, Y.; Zheng, M.; Qiao, X.; Jiang, B. Enhancing the strength and ductility in Mg-Zn-Ce alloy through achieving high density precipitates and texture weakening. *Adv. Eng. Mater.* **2017**, *19*, 1700487. [CrossRef]